63, 4, pp. 865–876, Warsaw 2025 https://doi.org/10.15632/jtam-pl/205901

INFLUENCE OF CONICAL STRUCTURE ON SEALING SPECIFIC PRESSURE UNDER STATIC LOADING

Chun LIU*, Luo Jin LI, Shu Wen HU

Laboratory of Science and Technology on Cryogenic Liquid Propulsion of CASC,
Beijing Aerospace Propulsion Institute, Beijing, China
*corresponding author, lchun1123@163.com

Similarity analysis and numerical simulations are performed to investigate the effects of axial force, material physical properties, and geometric shape of the conical structure on the sealing specific pressure. The results indicate that under a certain axial force, the conical structure can achieve a high sealing specific pressure. However, the sealing specific pressure decreases with the increase in the sealing surface diameter, sealing surface width, cone angle, and friction coefficient. In terms of material physical properties, the sealing specific pressure increases with the increase in Young's modulus of the upper cone, while other performance parameters have little effect on the sealing specific pressure. In addition, by using similarity analysis, a semi-empirical analytical expression model is proposed to represent the dependence of sealing specific pressure on the axial force, friction coefficient, material physical properties, and geometric properties of the conical structure.

Keywords: conical sealing structure; sealing specific pressure; similarity analysis; numerical simulation.



Articles in JTAM are published under Creative Commons Attribution 4.0 International. Unported License https://creativecommons.org/licenses/by/4.0/deed.en. By submitting an article for publication, the authors consent to the grant of the said license.

1. Introduction

Valves, as important components of process fluid systems, are widely used in industries, such as petroleum, chemical, aerospace, etc. Their sealing performance directly affects the effectiveness of the entire pipeline control system, which has been the focus of research (Deng et al., 2023; Chen et al., 2024). There are various types of valve seals, mainly including plane seals, spherical seals, curved seals, and conical seals. And with the development of numerical calculations, scholars have studied the influence of different factors on the sealing pressure of valves (Song & Zheng, 2013; Wang et al., 2024a; Kwak et al., 2019; Peng et al., 2021; Abbasov et al., 2021; Zhao et al., 2022; Yuvaraj & Arunkumar, 2025).

Li et al. (2023) conducted the sensitivity analysis of sealing structure parameters and determined the optimum size of the valve. The results show that the sealing performance of the valve was significantly improved after optimization. Yang et al. (2020) analyzed the influence of parameters such as the maximum interference fit and taper of the sealing ring contact surface on the sealing contact stress, and found that increasing the interference fit and taper is beneficial for improving the sealing performance. Wu et al. (2010) proposed a deep high-pressure conical valve based on a polyether ether ketone seat sealing structure and studied the sealing performance of the new valve. The results show that the new valve has better sealing performance. Jayanath et al. (2016) conducted a finite element analysis of the contact stress on nitrile rubber seals for valves, and their experimental results were found to be consistent with the finite element analysis results. Lin et al. (2022) analyzed the influence of sealing pair structure dimensions and medium pressure on sealing pressure. Wang et al. (2024b) propose a design scheme for an outer conical sealing structure to address the shortcomings of the conical sealing structure. The ad-

vantage of its sealing principle is that it not only ensures the sealing effect, but also reduces processing difficulty. Wu et al. (1992) analyzed the force state of the conical sealing pair and derived the relationship between the axial force and cone angle of the sealing pressure. However, this relationship ignores the fact that different conical sealing pairs will undergo different deformations under different axial forces, resulting in changes in the stress state. In addition, some researchers (Gorash et al., 2016; Romanik et al., 2019; Kwak et al., 2019; Li et al., 2024) have also conducted research on the design and performance of valve sealing structures, and obtained the sealing contact pressure under different working conditions.

In summary, researchers have made some progress in the design and performance of valve sealing structures. However, further research is needed on the sealing-specific pressure model of conical structures. On the one hand, although the theoretical formula for sealing specific pressure was established in early stages, the theoretical assumptions are too simplistic due to the deformation of the conical structure under axial force, resulting in significant deviations in calculations. On the other hand, previous simulation studies have only considered the influence of a small number of factors on the sealing specific pressure, making it difficult to obtain the functional relationship between the sealing specific pressure and various factors. Therefore, the purpose of this study is to investigate the quantitative dependence of sealing specific pressure on the axial force, friction coefficient, material physical properties, and geometric properties of the conical structure, so as to further guide the design of valve seal structure.

2. Similarity analysis of sealing specific pressure for conical structure

The sealing problem for a conical structure under axial force is illustrated in Fig. 1. When the upper cone is compressed against the lower cone by an axial force, the two cones undergo certain deformation and form a sealing surface with a certain sealing specific pressure, thereby achieving the sealing effect. In the following analysis, the sealing specific pressure for a conical structure under such axial force is derived using similarity analysis.

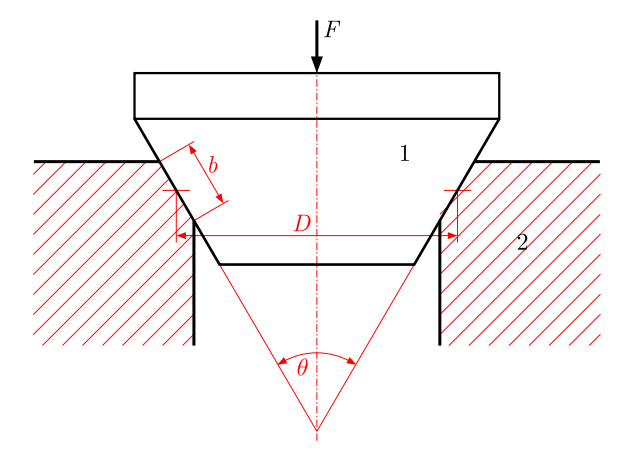


Fig. 1. Schematic diagram of conical structure: 1 – upper cone; 2 – lower cone.

Obviously, the specific sealing pressure for a conical structure depends on the axial force, the physical properties of material, and the geometric properties of the conical structure. Therefore, the sealing specific pressure p can be written as

$$p = f(F, D, b, \theta, \mu, E_1, E_2, v_1, v_2, \rho_1, \rho_2, \sigma_1, \sigma_2), \tag{2.1}$$

where F is the axial force, D is the sealing surface diameter, b is the sealing surface width, θ is the cone angle, μ is the friction coefficient, E_1 and v_1 are Young's modulus and Poisson's ratio of the lower cone, respectively. E_2 and v_2 are Young's modulus and Poisson's ratio of the upper

cone, respectively, ρ_1 and ρ_2 are the densities of the upper cone and lower cone, respectively, σ_1 and σ_2 are the yield strengths of the upper cone and lower cone, respectively.

The sealing problem for a conical structure under axial force is a static problem, so the inertia effect is not considered. The gravity of the upper cone is much smaller than the axial force, so the influence of cone gravity on the sealing specific pressure is negligible. In other words, it can be assumed that p is independent of ρ_1 and ρ_2 . Additionally, to ensure the strength reliability of the conical sealing structure, the stresses on both cones should be less than the yield strength of the materials, so the yield strength has almost no effect on the change in the sealing specific pressure, which means that p can be regarded as independent of σ_1 and σ_2 . Therefore, Eq. (2.1) can be simplified as

$$p = f(F, D, b, \theta, \mu, E_1, E_2, v_1, v_2). \tag{2.2}$$

In the conical sealing structure, Young's modulus of the lower cone is larger than that of the upper cone. When the upper cone is compressed against the lower cone by axial force, the upper cone undergoes more deformation than the lower cone, causing the area of the contact surface to change, which is consistent with the subsequent simulation results. The changes in Young's modulus and Poisson's ratio of the lower cone in a certain range have little effect on the deformation and thus on the area of the contact surface. Therefore, the influence of Young's modulus and Poisson's ratio for the lower cone on the specific sealing pressure can be ignored. Equation (2.2) can be rewritten as

$$p = f(F, D, b, \theta, \mu, E_2, v_2). \tag{2.3}$$

According to Barenblatt (1996), in the MLT (corresponding to mass, length, and time) class of systems of units, the dimension of each quantity involved in Eq. (2.3) can be defined as follows:

$$\dim p = ML^{-1}T^{-2},$$
 $\dim F = MLT^{-2},$ $\dim D = \dim b = L,$ $\dim \theta = \dim \mu = 1,$ (2.4)
$$\dim E_2 = ML^{-1}T^{-2},$$
 $\dim v_2 = 1.$

It is straightforward to verify that the dimensions of F and D are independent. By considering these two variables as the basic system determining the independent variable, the remaining dependent variables in Eq. (2.4) can be expressed as

$$\dim p = \dim (F/D^2), \qquad \dim b = \dim D,$$

$$\dim \mu = \dim \theta = \dim v_2 = 1,$$

$$\dim E_2 = \dim (F/D^2).$$
(2.5)

Therefore, by using the Buckingham Pi theorem, Eq. (2.3) can be written in the following dimensionless form:

$$\Pi = f(\Pi_1, \Pi_2, \Pi_3, \Pi_4, \Pi_5), \tag{2.6}$$

where f is an arbitrary function and

$$\Pi = \frac{p}{F/D^2},$$

$$\Pi_1 = \frac{b}{D}, \qquad \Pi_2 = \theta, \qquad \Pi_3 = \mu, \qquad \Pi_4 = \frac{E_2}{F/D^2}, \qquad \Pi_5 = v_2.$$
(2.7)

By substituting Eq. (2.7) into Eq. (2.6), we get

$$\frac{p}{F/D^2} = f\left(\frac{b}{D}, \theta, \mu, \frac{E_2}{F/D^2}, v_2\right). \tag{2.8}$$

One can see that there are now five dimensionless arguments in Eq. (2.8), which can be simplified further by using incomplete similarity or the second type of self-similarity (Barenblatt, 1996).

First, the dimensionless parameter Π_1 is analyzed. The sealing surface width used in this study is b=0.4–2 mm, the sealing surface diameter is D=4–20 mm, and there is $\Pi_1=0.02$ –0.5. Moreover, when other parameters remain constant, the larger the sealing surface width b, the larger the contact area between the two conical surfaces, and the smaller the sealing specific pressure p. According to Barenblatt (1996), in traditional "physical level" discussions, the parameter Π_1 should be considered essential. This indicates that Π may have incomplete self-similarity or similarity of the second type in the dimensionless parameter Π_1 . In other words, assuming that a function f_1 has an arbitrary power law-type asymptotic expression, Eq. (1.6) can be written in the following simplified form:

$$\Pi = \Pi_1^{\alpha} f_1(\Pi_2, \Pi_3, \Pi_4, \Pi_5), \tag{2.9}$$

where α is an undetermined constant exponent.

Secondly, regarding the dimensionless parameter Π_2 and Π_3 , we have $\Pi_2 = 50^{\circ}-90^{\circ}$ and $\Pi_3 = 0.3-0.38$ in this study. According to the force analysis of the conical sealing structure, it can be concluded that for Π_2 , when other parameters remain constant, as the cone angle increases, the normal stress on the contact surface decreases and the sealing specific pressure decreases, which is consistent with the subsequent simulation results; for Π_3 , when other parameters remain constant, as the cone angle increases, the normal stress on the contact surface decreases and the sealing specific pressure decreases, which is consistent with the subsequent simulation results. As in the analysis for Π_1 , Π has incomplete self-similarity or similarity of the second type in the dimensionless parameters Π_2 and Π_3 . Therefore, Eq. (2.9) can be written in the following simpler form:

$$\Pi = \Pi_1^{\alpha} \, \Pi_2^{\beta} \, \Pi_3^{\gamma} \, f_2 \, (\Pi_4, \Pi_5), \tag{2.10}$$

where f_2 is an arbitrary function, and α , β , γ are three undetermined constant exponents.

Finally, regarding the dimensionless parameter Π_4 , with $F = 200 \,\mathrm{N}$, $E_2 = 2.67 \,\mathrm{GPa}$, and $D = 8 \,\mathrm{mm}$, we have $\Pi_4 = 854$, which is much greater than 10. However, when Young's modulus E_2 decreases within a certain range, the increase in contact area leads to an increase in the sealing specific pressure p, which will not approach a constant. According to Barenblatt (1996), this indicates that Π may have incomplete self-similarity or similarity of the second type in the dimensionless parameter Π_4 . Then Eq. (2.10) can be expressed as

$$\Pi = \Pi_1^{\alpha} \, \Pi_2^{\beta} \, \Pi_3^{\gamma} \, \Pi_4^{\eta} \, f_3 \, (\Pi_5), \tag{2.11}$$

where f_3 is an arbitrary function, and α , β , γ , η are four undetermined constant exponents. Substituting Eq. (2.7) into Eq. (2.11) yields

$$\frac{p}{F/D^2} = \left(\frac{b}{D}\right)^{\alpha} \theta^{\beta} \mu^{\gamma} \left(\frac{E_2}{F/D^2}\right)^{\eta} f_3(v_2). \tag{2.12}$$

The function $f_3(v_2)$ and the four undetermined constant exponents α , β , γ , η will be determined based on the following numerical results.

3. Numerical simulation

3.1. Simulation model

The sealing specific pressure of the conical structure under axial force was investigated using ANSYS-WORKBENCH. The conical structure is an axisymmetric structure, so the model is simplified to a $^{1}/^{2}$ model. The upper cone material is aluminum alloy 2A14. The lower cone material is 20 Cr13, and the physical properties of the material are shown in Table 1. Additionally, grid partitioning is a crucial step in simulation analysis, where grid quality has a significant impact on the accuracy and precision of the simulation analysis. In order to ensure sufficient accuracy of the calculation results, the mesh of the contact area was encrypted with a mesh size of $0.02\,\mathrm{mm}$, as shown in Fig. 2a. The contact surface is set to frictional contact. The bottom boundary of the lower cone is set as a fixed support to prevent the lower cone from moving. The displacement constraint of the upper cone surface in the X- and Z-directions is $0\,\mathrm{mm}$, and only axial movement is allowed. Axial force is applied to the upper cone surface to ensure sealing, as shown in Fig. 2b.

Table 1. Physical properties of material.

Material	$\rho [\mathrm{kg/m^3}]$	E [GPa]	v	σ_s [MPa]
2A14	2800	72	0.33	380
20Cr13	7750	200	0.3	540

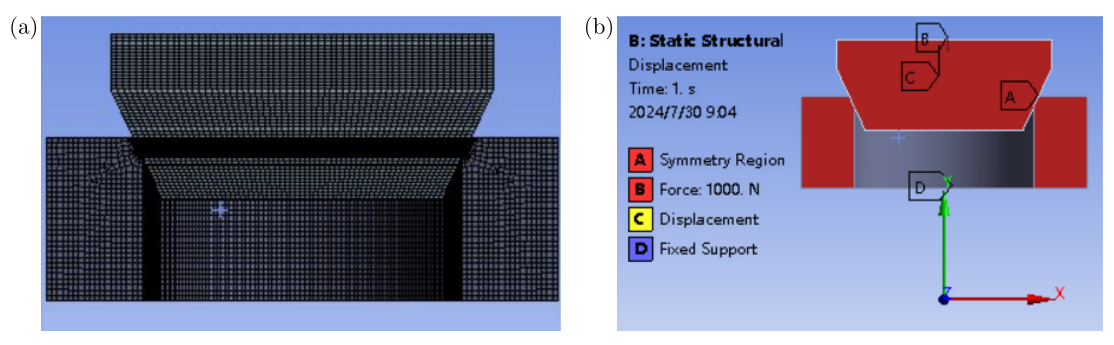


Fig. 2. Simulation model of cone seal structure: (a) grid distribution; (b) boundary conditions.

3.2. Numerical results and discussion

3.2.1. Dependence of sealing specific pressure on axial force

To study the effects of axial force on sealing specific pressure, for an axial force range of 500 N to 2000 N, we numerically simulated a conical structure with a diameter of $D=12\,\mathrm{mm}$, width of $b=0.8\,\mathrm{mm}$, and angle of $\theta=50^\circ$. In all of these numerical simulations, the friction coefficient was $\mu=0.2$.

Figure 3 shows the equivalent stress distribution of the conical structure under an axial force $F = 2000 \,\mathrm{N}$. In Fig. 3, it can be seen that the maximum equivalent stresses of the upper and

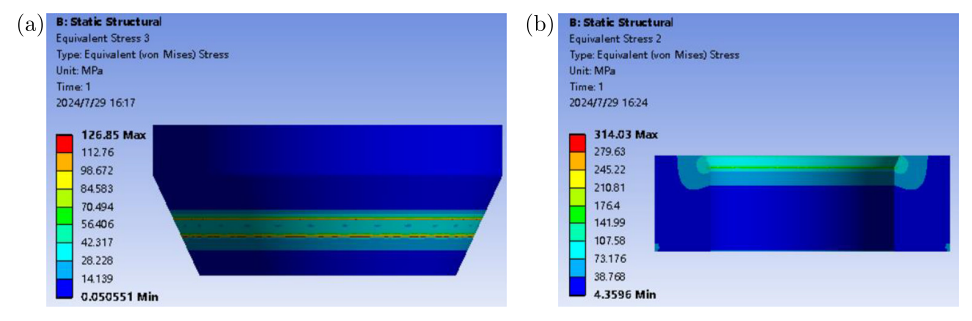


Fig. 3. Equivalent stress distribution of conical sealing structure: (a) upper cone; (b) lower cone.

lower cones are $126.8\,\mathrm{MPa}$ and $314\,\mathrm{MPa}$, respectively, both of which are lower than the yield strength of the material. In addition, the equivalent stress in the middle part of the contact surface is relatively small, while the equivalent stress in the upper and lower boundary parts is relatively large. Figure 4 shows the equivalent strain distribution of the conical structure under an axial force $F = 2000\,\mathrm{N}$. In Fig. 4, it can be seen that the maximum strains of the upper and lower cones are $0.0018\,\mathrm{mm/mm}$ and $0.0016\,\mathrm{mm/mm}$, respectively, and the deformation of the upper conical surface is relatively large. Figure 5 shows the sealing-specific pressure distribution on the sealing contact surface under an axial force of $F = 2000\,\mathrm{N}$. In Fig. 5, it can be seen that the sealing specific pressure of the conical structure is relatively small in the middle of the sealing band, with the highest values at the upper and lower boundary positions, about 298 MPa, and the positions of the maximum stress and maximum deformation correspond to the positions of the maximum sealing specific pressure.

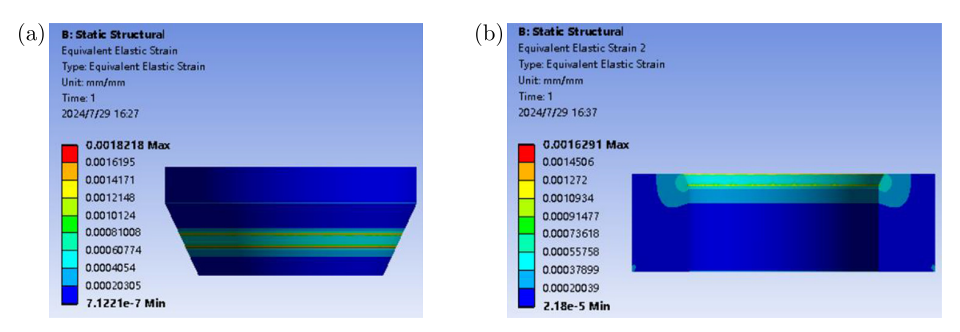


Fig. 4. Strain distribution of conical sealing structure: (a) upper cone; (b) lower cone.

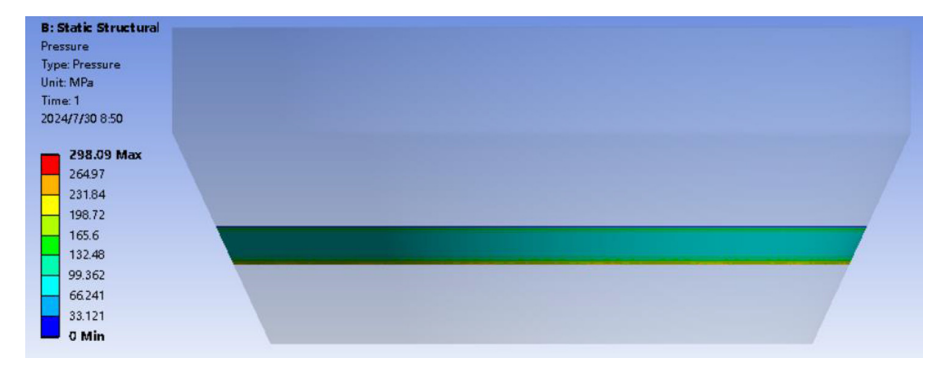


Fig. 5. Sealing specific pressure on the contact surface.

To obtain a general rule for the dependence of the sealing specific pressure on the axial force, additional numerical simulations with various values of F were conducted. The numerical results are presented in Table 2. One can observe that with an increase in the axial force, the stress and sealing specific pressure of the conical structure also increase. Under the action of the axial force $F = 2500 \,\mathrm{N}$, the stress of the conical structure with $D = 12 \,\mathrm{mm}$, $b = 0.8 \,\mathrm{mm}$, and $\theta = 50^{\circ}$ is less than the yield strength of the material, indicating high reliability.

F[N]	Upper cone stress [MPa]	Lower cone stress [MPa]	p [MPa]
500	36.7	99.1	87.7
1000	67.2	184.4	162.2
1500	98.1	270.1	236.6
2000	126.8	314.0	298.1

178.3

2500

Table 2. Sealing specific pressure of conical sealing structure under different axial forces.

367.4

355.4

3.2.2. Dependence of sealing specific pressure on sealing surface diameter

To study the effects of the sealing surface diameter on sealing specific pressure, numerical simulations for conical sealing structures with various sealing surface diameters ($D=4\,\mathrm{mm}$, 8 mm, 12 mm, 16 mm, and 20 mm) were conducted with the width of $b=0.8\,\mathrm{mm}$, and angle of $\theta=70^\circ$. In all of these numerical simulations, the axial force was $F=2000\,\mathrm{N}$ and the friction coefficient was $\mu=0.2$.

The sealing specific pressure for different sealing diameters is shown in Table 3. According to Table 3, as the sealing surface diameter increases, the stress and sealing specific pressure of the conical structure gradually decrease. The sealing specific pressure of the conical structure with a sealing surface diameter of $D=4\,\mathrm{mm}$ is the highest, at 640 MPa, which is 3.1 times the sealing specific pressure of the conical structure with a sealing surface diameter of $D=20\,\mathrm{mm}$. This is because, under the same axial force, a smaller sealing surface diameter results in a smaller contact area, leading to a higher sealing specific pressure.

D [mm]	Upper cone stress [MPa]	Lower cone stress [MPa]	p [MPa]
4	294.4	627.0	660.0
8	145.8	325.3	371.0
12	99.2	227.5	264.9
16	80.0	183.8	221.9
20	69.6	163.5	205.6

Table 3. Sealing specific pressure of conical structures with different sealing surface diameters.

3.2.3. Dependence of sealing specific pressure on sealing surface width

To study the effects of the sealing surface width on sealing specific pressure, numerical simulations for conical structures with various sealing surface widths ($b=0.4\,\mathrm{mm}$, $0.8\,\mathrm{mm}$, $1.2\,\mathrm{mm}$, $1.6\,\mathrm{mm}$, and $2\,\mathrm{mm}$) were conducted with a diameter of $D=0.8\,\mathrm{mm}$, and an angle of $\theta=70^\circ$. In all of these numerical simulations, the axial force was $F=2000\,\mathrm{N}$ and the friction coefficient was $\mu=0.2$.

The numerical results of sealing specific pressure for conical structures with different sealing surface widths are shown in Table 4. In Table 4, one can see that as the sealing surface width increases, the stress and sealing specific pressure of the conical structure gradually decrease. This is because under the same axial force, a smaller sealing surface width will result in a smaller contact area, leading to a higher sealing specific pressure.

b [mm]	Upper cone stress [MPa]	Lower cone stress [MPa]	p [MPa]
o [mm]	opper cone stress [wir a]	Lower cone stress [wir a]	p [MII a]
0.4	138.8	326.4	348.7
0.8	99.2	227.5	264.9
1.2	84.2	214.5	223.6
1.6	75.6	173.6	207.4
2	68.9	160.1	195.6

Table 4. Sealing specific pressure of conical structures with different sealing surface widths.

3.2.4. Dependence of sealing specific pressure on cone angle

To study the effects of the cone angle on sealing specific pressure, numerical simulations for conical structures with various cone angles ($\theta = 50^{\circ}, 60^{\circ}, 70^{\circ}, 80^{\circ}, \text{ and } 90^{\circ}$) were conducted with

the diameter of $D = 0.8 \,\mathrm{mm}$, and width of $b = 12 \,\mathrm{mm}$. In all of these numerical simulations, the axial force was $F = 2000 \,\mathrm{N}$ and the friction coefficient was $\mu = 0.2$.

The numerical results of sealing specific pressure for conical structures with different cone angles are shown in Table 5. According to Table 5, the stress and sealing specific pressure of the conical structure gradually decrease with the increase in the cone angle. This is because under the same axial force, the increase in the cone angle reduces the normal stress on the contact surface, resulting in a decrease in sealing specific pressure, which is consistent with the theoretical analysis results.

θ [°]	Upper cone stress [MPa]	Lower cone stress [MPa]	$p \; [\mathrm{MPa}]$
50	126.8	314.1	298.1
60	111.2	284.1	286.5
70	99.2	227.5	264.9
80	89.2	218.2	246.2
90	81.3	209.1	235.6

Table 5. Sealing specific pressure of conical structures with different cone angles.

3.2.5. Dependence of sealing specific pressure on friction coefficient

To study the effects of the friction coefficient on sealing specific pressure, numerical simulations for conical sealing structures with various friction coefficients ($\mu = 0.1, 0.2, 0.3, 0.4$, and 0.5) were conducted with a diameter of D = 0.8 mm, a cone angle of $\theta = 50^{\circ}$, and a width of b = 8 mm. In all of these numerical simulations, the axial force was F = 2000 N.

The numerical results of sealing specific pressure for conical structures with different friction coefficients are shown in Table 6. According to Table 6, the stress and sealing specific pressure of the conical structure gradually decreases with the increase in the friction coefficient. This is because under the same axial force, the increase in the friction coefficient reduces the normal stress on the contact surface, resulting in a decrease in sealing specific pressure, which is consistent with the theoretical analysis results.

μ	Upper cone stress [MPa]	Lower cone stress [MPa]	p [MPa]
0.1	157.2	361.3	336.2
0.2	126.8	314.0	298.0
0.3	128.3	328.9	270.7
0.4	130.5	308.6	240.1
0.5	135.7	291.7	215.4

Table 6. Sealing specific pressure of conical structures with different friction coefficients.

3.2.6. Dependence of sealing specific pressure on Young's modulus and Poisson's ratio

To study the effects of Young's modulus and Poisson's ratio on sealing specific pressure, numerical simulations for conical sealing structures were conducted with the diameter of $D=0.8\,\mathrm{mm}$, cone angle of $\theta=50^\circ$, and width of $b=8\,\mathrm{mm}$. In all of these numerical simulations, the axial force was $F=2000\,\mathrm{N}$ and the friction coefficient was $\mu=0.2$.

The influence of Young's modulus ($E_2 = 100 \,\text{GPa}$, 120 GPa, 150 GPa, 180 GPa, and 200 GPa) of the upper cone on the sealing specific pressure was first analyzed. The numerical results of sealing specific pressure for different Young's modulus of the upper cone are shown in Table 7. According to Table 7, the sealing specific pressure of the conical structure gradually increases

E_2 [GPa]	Upper cone stress [MPa]	Lower cone stress [MPa]	p [MPa]
100	135.8	370.8	325.6
120	139.6	377.8	333.6
150	144.9	389.2	347.5
180	150.0	399.4	358.3
200	153.2	405.7	364.8

Table 7. Sealing specific pressure of conical structures with different Young's modulus.

with the increase in Young's modulus of the upper cone. This is because under the same axial force, the increase in Young's modulus of the upper cone causes less deformation, resulting in a smaller contact area and an increase in sealing specific pressure. In addition, the influence of Poisson's ratio ($v_2 = 0.3, 0.32, 0.34, 0.36, \text{ and } 0.38$) of the upper cone on the sealing specific pressure was analyzed. The numerical results of sealing specific pressure for different Poisson's ratios are shown in Table 8. According to Table 8, with the increase in Poisson's ratio of the upper cone, the change in sealing specific pressure is relatively small, at approximately 4 MPa, which can be almost ignored.

v_2	Upper cone stress [MPa]	Lower cone stress [MPa]	p [MPa]
0.3	156.9	407.1	366.2
0.32	154.4	406.2	365.3
0.34	152.0	405.2	364.4
0.36	149.8	404.1	363.5

Table 8. Sealing specific pressure of conical structures with different Poisson's ratio.

4. Semi-empirical analytical expression for sealing specific pressure

403.1

362.6

To determine the model constants α , β , γ , η , and the function $f_3(v_2)$ in Eq. (2.12), the numerical results derived above are used. Numerical fitting of these numerical results will be conducted using the Levenberg-Marquardt optimization algorithm.

Firstly, in Table 8, one can see that within a certain range, the change in Poisson's ratio of the upper cone has a relatively small impact on the sealing specific pressure and can be ignored. Therefore, when other parameters (axial force, sealing surface diameter, sealing surface width, cone angle, friction coefficient, Young's modulus of upper cone) remain unchanged, $f_3(v_2)$ can be written in the following form:

$$f_3(v_2) = c,$$
 (4.1)

where c is a constant. Therefore, substituting Eq. (4.1) into Eq. (2.12) yields

147.7

0.38

$$\frac{p}{F/D^2} = c \left(\frac{b}{D}\right)^{\alpha} \theta^{\beta} \mu^{\gamma} \left(\frac{E_2}{F/D^2}\right)^{\eta}. \tag{4.2}$$

The parameters in Eq. (4.2) were determined by fitting the above simulation results. The fitting results and model parameters are shown in Fig. 6 and Table 9, respectively. Therefore, the sealing specific pressure of the conical structure can ultimately be expressed as

$$p = \frac{0.72F^{0.79}E_2^{0.21}}{D^{1.12}b^{0.46}\theta^{0.44}\mu^{0.25}}. (4.3)$$

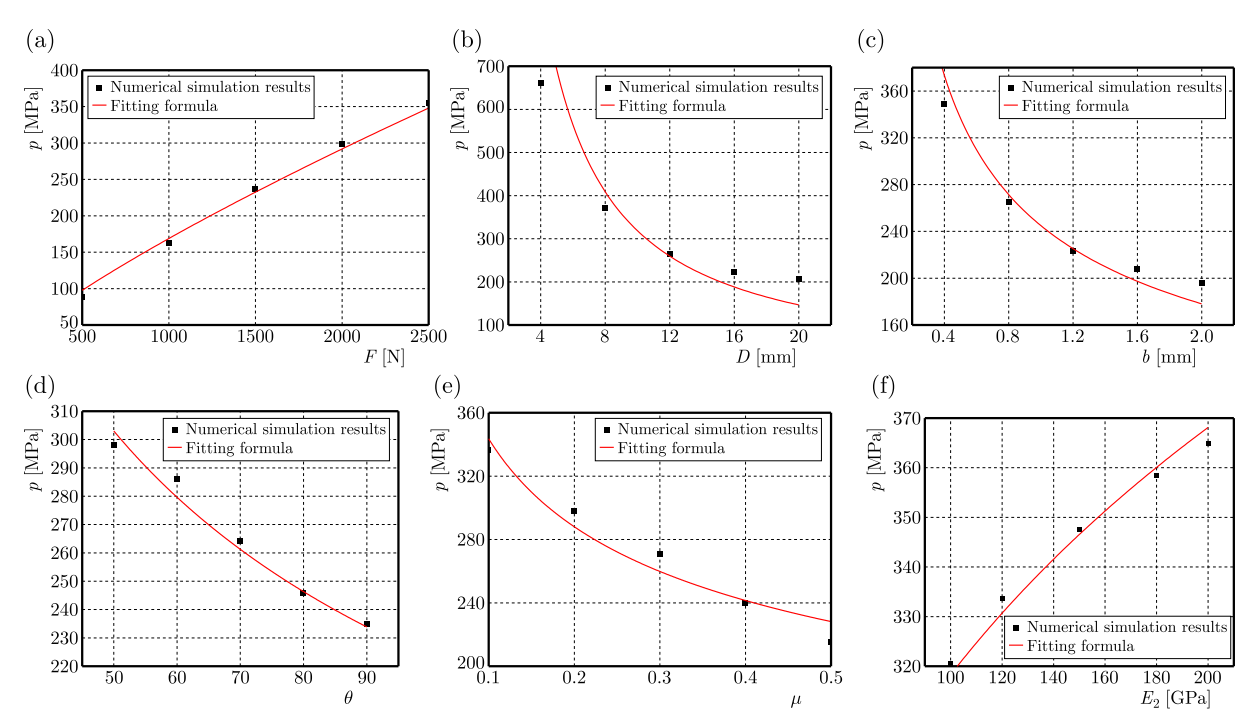


Fig. 6. Sealing specific pressure versus (a) axial force, (b) sealing surface diameter, (c) sealing surface width, (d) cone angle, (e) friction coefficient, and (f) Young's modulus.

Table 9. Parameters of the model.

c	α	β	γ	η
0.72	-0.46	-0.44	-0.25	0.21

5. Conclusions

In this study, similarity analysis and numerical simulations were conducted on the relationship between the sealing specific pressure and various factors for the conical structure under axial loading, specifically involving axial force, cone angle, sealing surface width, sealing surface diameter, and physical properties of materials. The main conclusions are as follows:

- 1) based on the similarity theory, a semi-empirical analytical expression for the sealing specific pressure of the conical structure was obtained, which can well predict the dependence of the sealing specific pressure on axial force, material physical properties, and the geometric shape of the conical structure (cone angle, sealing surface width, sealing surface diameter);
- 2) in addition to the influence of the geometric shape of the conical structure on the sealing specific pressure, the friction coefficient also has a significant impact on the sealing specific pressure, which requires us to ensure that the conical surface has appropriate roughness when being processed;
- 3) in the metal conical structure, Young's modulus of the upper cone has a significant impact on the sealing specific pressure, which has guiding significance for the selection of conical structure materials.

References

1. Abbasov, E.M., Rustamova, K.O., & Darishova, A.O. (2021). Influence of viscous-elastic properties of a cylindrical sealing element on its sealing ability. *Journal of Theoretical and Applied Mechanics*, 59(3), 481–492. https://doi.org/10.15632/jtam-pl/140228

- 2. Barenblatt, G.I. (1996). Scaling, self-similarity, and intermediate asymptotics. Cambridge University Press. https://lab.semi.ac.cn/library/upload/files/2021/8/30133839528.pdf
- 3. Chen, Y.Q., Yu, H., Fu, S.W., & Li, A. (2024). Study on sealing performance of main gate valve of marine nuclear power plant based on fluid-solid-thermal coupling method. Frontiers in Energy Research, 12, Article 1375806. https://doi.org/10.3389/fenrg.2024.1375806
- 4. Deng, C., Nie, J., Luo, L., Wang, B., Chen, G., Wu, S., Shi, Y., Shi, J., Gao, W., Liu, S., & Zhang, W. (2023). Experimental analysis of the effect of sealing surface pitting defects on valve sealing performance. In H. Dong, & H. Yu (Eds.). Proceedings: Vol. 12801. Ninth International Conference on Mechanical Engineering, Materials, and Automation Technology (MMEAT 2023) (Article 128011V). SPIE. https://doi.org/10.1117/12.3007569
- 5. Gorash, Y., Dempster, W., Nicholls, W.D., Hamilton, R., & Anwar, A.A. (2016). Study of mechanical aspects of leak tightness in a pressure relief valve using advanced FE-analysis. *Journal of Loss Prevention in the Process Industries*, 43, 61–74. https://doi.org/10.1016/j.jlp.2016.04.009
- Jayanath, S., Achuthan, A., Mashue, A., & Huang, M. (2016). A subscale experimental test method to characterize extrusion-based elastomer seals. *Journal of Tribology*, 138(3), Article 032201. https://doi.org/10.1115/1.4032175
- Kwak, H.-S., Seong, H., & Kim, C. (2019). Design of laminated seal in cryogenic triple-offset butterfly valve used in LNG marine engine. *International Journal of Precision Engineering and Manufacturing*, 20(2), 243–253. https://doi.org/10.1007/s12541-019-00056-6
- 8. Li, S., Kang, W., Liu, T., Yang, L., & Wang, Y. (2023). Sealing structure optimization of LNG ultra-low temperature and high-pressure axial flow check valve. *Journal of Applied Science and Engineering*, 26(7), 1013–1024. https://doi.org/10.6180/jase.202307_26(7).0012
- 9. Li, S.X., Zheng, M.X., Wang, Y.X., Yang, L.X., & Ma, T.Q. (2024). Multi-objective optimization design of double resilient groove metal seat for ball valve in liquid hydrogen receiving stations. *Journal of the Brazilian Society of Mechanical Sciences and Engineering*, 46(1), Article 34. https://doi.org/10.1007/s40430-023-04602-2
- 10. Lin, Z.-H., Yu, L.-J., Hua, T.-F., Jin, Z.-J., & Qian, J.-Y. (2022). Seal contact performance analysis of soft seals on high-pressure hydrogen charge valves. *Journal of Zhejiang University-SCIENCE A* (Applied Physics & Engineering), 23(4), 247–256. https://doi.org/10.1631/jzus.A2100395
- 11. Peng, C., Fischer, F.J., Schmitz, K., & Murrenhoff, H. (2021). Comparative analysis of leakage calculations for metallic seals of ball-seat valves using the multi-asperity model and the magnification-based model. *Tribology International*, 163, Article 107130. https://doi.org/10.1016/j.triboint.2021. 107130
- 12. Romanik, G., Jaszak, P., & Rogula, J. (2019). Cooperation of the PTFE sealing ring with the steel ball of the valve subjected to durability test. *Open Engineering*, 9(1), 321–328. https://doi.org/10.1515/eng-2019-0028
- 13. Song, R., & Zheng, F. (2013). Analysis of ball valve sealing pressure ratio based on UG Nastran. Advanced Materials Research, 703, 204–207. https://doi.org/10.4028/www.scientific.net/AMR.703.204
- 14. Wang, C.L., Xu, D.T., Huang, K.X., Liu, Y., & Yang, L. (2024a). Multi-objective optimization of a triple-eccentric butterfly valve considering structural safety and sealing performance. *ISA Transactions*, 155, 295–308. https://doi.org/10.1016/j.isatra.2024.10.009
- 15. Wang, X., Cao, J., Yang, B., & Wu, X.-J. (2024b). Design and application of a new sealing structure (in Chinese). $Hydraulics\ Pneumatics\ &\ Seals,\ 44$ (12), 118–122. https://doi.org/10.3969/j.issn.1008-0813.2024.12.019
- 16. Wu, H.J., Guo, B.Z., & Ding, Y.R. (1992). Theoretical discussion on the selection of cone angle of valve cone sealing (in Chinese). *Fluid Machinery*, 09, 22–24.
- 17. Wu, S.-J., Yang, C.-J., Chen, Y., & Xie, Y.-Q. (2010). A study of the sealing performance of a new high-pressure cone valve for deep-sea gas-tight water samplers. *Journal of Pressure Vessel Technology*, 132(4), Article 041601. https://doi.org/10.1115/1.4001204

18. Yang, Y.W., Zhu, H.W., He, D.S., Du, C.C., Xu, L.B., He, Y., Zheng, Y., & Ye, Z.W. (2020). Contact mechanical behaviors of radial metal seal for the interval control valve in intelligent well: Modeling and theoretical study. *Energy Science & Engineering*, 8(4), 1337–1352. https://doi.org/10.1002/ese3.597

- 19. Yuvaraj, K., & Arunkumar, G. (2025). Simulation and validation of the effect of hydrostatic and non-hydrostatic pressure on contact pressure in a resilient seat butterfly valve. *Materials Research Express*, 12(1), Article 016511. https://doi.org/10.1088/2053-1591/ada877
- 20. Zhao, B., Zhang, S., Gao, Q., Miao, C., & Wang, T. (2022). Optimization of sealing parameters of double-sealing pipeline repair clamp. *Journal of Theoretical and Applied Mechanics*, 60(3), 333–346. https://doi.org/10.15632/jtam-pl/150679

Manuscript received April 10, 2025; accepted for publication June 4, 2025; published online October 28, 2025.